

Low-Frequency Excitation of Singlet-Triplet Transitions. Application to Nuclear Hyperpolarization

Laurynas Dagens,¹ Christian Bengs,¹ and Malcolm H. Levitt¹
Department of Chemistry, University of Southampton, SO17 1BJ, UK

(*Electronic mail: mhl@soton.ac.uk)

(Dated: 8 September 2021)

Coupled pairs of nuclear spins-1/2 support one singlet state and three triplet states. Transitions between the singlet state and one of the triplet states may be driven by an oscillating low-frequency magnetic field, in the presence of couplings to a third nuclear spin, and a weak bias magnetic field. The oscillating field is in the same direction as the bias field, and is called a WOLF (Weak Oscillating Low Field) pulse. Application of a WOLF pulse allows the generation of strong nuclear hyperpolarization of ¹³C nuclei, starting from the nuclear singlet polarization of a ¹H spin pair, associated with the enriched para spin isomer of hydrogen gas. Hyperpolarization is demonstrated for two molecular systems.

I. INTRODUCTION

Magnetic resonance experiments usually involve the application of a strong magnetic field (typically, from a fraction of one Tesla up to tens of Tesla) combined with radiofrequency pulses (for nuclear magnetic resonance, NMR) or microwave pulses (for electron spin resonance, ESR) that are resonant with the magnetic Zeeman transitions of the system. In these high-field conditions, the parts of the spin Hamiltonian that do not commute with the Zeeman Hamiltonian are usually removed. This *secular approximation* leads to a major simplification of spin dynamical theory and is one of the cornerstones of modern NMR theory¹. One consequence is that all transitions involving combinations or multiples of the Larmor frequencies are not observed in NMR or ESR spectra. Some exceptions to this paradigm exist, such as ‘‘overtone’’ transitions in the NMR of nuclei with large quadrupolar moments², and the use of non-secular hyperfine couplings in solid-effect dynamic nuclear polarization³ and stimulated nuclear polarization⁴.

In the case of NMR, the secular approximation breaks down in very small magnetic fields, such that the Larmor frequencies are comparable in magnitude to the spin-spin interactions⁵. Here we show that the mixing of states by non-secular spin-spin couplings in the low-field regime allows selected ‘‘forbidden’’ transitions to be induced by oscillating magnetic fields. In suitable circumstances, this phenomenon allows the generation of strong hyperpolarization in the reaction products of hydrogen gas enriched in the *para* spin isomer. We demonstrate the generation of two small molecules in solution with high levels of ¹³C polarization. One of these substances, fumarate, is a natural metabolite which has been used for the characterisation of cancer in magnetic resonance imaging (MRI)⁶.

II. THEORY

Consider an ensemble of nuclear three-spin-1/2 systems, each consisting of two nuclei I_1 and I_2 of one isotopic type with magnetogyric ratio γ_I , and a third nucleus S_3 of a different isotopic type with magnetogyric ratio γ_S . In the isotropic

solution state, the three nuclei mutually interact by scalar spin-spin coupling terms mediated by the bonding electrons. These couplings consist of a homonuclear coupling J_{12} , and two heteronuclear couplings J_{13} and J_{23} . The two heteronuclear couplings are assumed to be different, $J_{13} \neq J_{23}$. In the absence of any external fields the Hamiltonian of such a configuration is given by

$$H_J = 2\pi J_{12} \mathbf{I}_1 \cdot \mathbf{I}_2 + 2\pi J_{13} \mathbf{I}_1 \cdot \mathbf{I}_3 + 2\pi J_{23} \mathbf{I}_2 \cdot \mathbf{I}_3. \quad (1)$$

The presence of external magnetic fields is incorporated by coupling the individual spin angular momenta to the external magnetic field taking their respective gyromagnetic ratios into account. For an I_2S spin system the magnetic Hamiltonian is as follows:

$$H_M(t) = -\gamma_I \mathbf{B}(t) \cdot (\mathbf{I}_1 + \mathbf{I}_2) - \gamma_S \mathbf{B}(t) \cdot \mathbf{I}_3. \quad (2)$$

so that the total spin Hamiltonian is given by

$$H(t) = H_J + H_M(t). \quad (3)$$

A. WOLF pulses

Consider now the application of a small magnetic field B_z along the laboratory frame z -axis. For a WOLF pulse we may represent this field as the sum of a time-independent ‘‘bias’’ field B_{bias} , and a time-dependent oscillating field denoted B_{WOLF}

$$B_z(t) = B_{\text{bias}} + B_{\text{WOLF}}(t). \quad (4)$$

The oscillating field is explicitly given by

$$B_{\text{WOLF}}(t) = B_{\text{WOLF}}^0 \cos(\omega_{\text{WOLF}} t), \quad (5)$$

where ω_{WOLF} is the frequency of the oscillating field, and B_{WOLF}^0 is its peak amplitude. Since the applied oscillating field is small in magnitude and low in frequency, we refer to the oscillating magnetic field as a WOLF (*Weak Oscillating Low Frequency*) pulse.

Note that the B_{bias} and B_{WOLF} fields are applied in the *same direction*. This geometry differs from most NMR experiments, where oscillating fields are applied transverse to the

main field, with few exceptions^{2,7,8}. The Hamiltonian describing the interaction with the externally applied fields therefore reduces to

$$H_M(t) = -\gamma I B_z(t)(I_{1z} + I_{2z}) - \gamma_S B_z(t)S_z. \quad (6)$$

If the magnetic fields are low enough that chemical shifts are negligible, the spin Hamiltonian may be decomposed as a sum of five terms

$$\begin{aligned} H(t) &= H_J + H_M(t) \\ &= H_A + H_B + H_C + H_D + H_{\text{WOLF}}(t). \end{aligned} \quad (7)$$

The individual contributions are given by

$$\begin{aligned} H_A &= -B_{\text{bias}}(\gamma(I_{1z} + I_{2z}) + \gamma_S S_{3z}) \\ &\quad + 2\pi J_{12} \mathbf{I}_1 \cdot \mathbf{I}_2 + \pi(J_{13} + J_{23})(I_{1z} + I_{2z})S_{3z}, \\ H_B &= \pi(J_{13} - J_{23})(I_{1z} - I_{2z})S_{3z}, \\ H_C &= \frac{1}{2}\pi(J_{13} + J_{23}) \\ &\quad \times (I_1^+ S_3^- + I_2^+ S_3^- + I_1^- S_3^+ + I_2^- S_3^+), \\ H_D &= \frac{1}{2}\pi(J_{13} - J_{23}) \\ &\quad \times (I_1^+ S_3^- - I_2^+ S_3^- + I_1^- S_3^+ - I_2^- S_3^+), \\ H_{\text{WOLF}}(t) &= -B_{\text{WOLF}}(t)(\gamma(I_{1z} + I_{2z}) + \gamma_S S_{3z}). \end{aligned} \quad (8)$$

The terms H_A , H_C , and H_{WOLF} are symmetric with respect to exchange of the two I -spins, while the terms H_B and H_D are antisymmetric. If the Larmor frequency of the nuclei in the bias field is larger than the spin-spin couplings, and the difference between the heteronuclear couplings is smaller than the homonuclear coupling ($|J_{13} - J_{23}| \ll |J_{12}|$, i.e. near-equivalence⁹), then the H_A term dominates. The terms H_C and H_{WOLF} commute with H_A and may be regarded as secular, while the terms H_B and H_D do not commute with H_A and are non-secular. The terms H_B and H_C both give rise to small eigenvalue shifts, which are neglected here, for the sake of

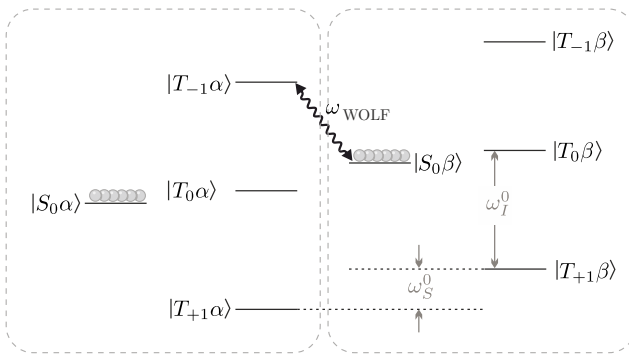


FIG. 1. Eigenvalues and eigenstates of H_A (equation 8) for a system of two I -spins and one S -spin, in the near-equivalence limit ($|J_{13} - J_{23}| \ll |J_{12}|$). The circles represent the population distribution for a fully populated singlet state between the two I -spins. The Larmor frequencies in the bias field B_{bias} are indicated: $\omega_I^0 = -\gamma B_{\text{bias}}$ for the I -spins, and $\omega_S^0 = -\gamma_S B_{\text{bias}}$ for the S -spins. The WOLF pulse is applied with a frequency ω_{WOLF} matching the transition frequency ω_{ST} between the indicated pair of states (equation 12).

brevity. The exchange-antisymmetric non-secular term H_D is the most important one for the purposes of this paper. The eigenstates and eigenvalues of H_A are sketched in figure 1. The eigenstates are direct products of the singlet and triplet states of the I -spin pair with the Zeeman states of the S -spin, such that the triplet product states are symmetric and the singlet product states are anti-symmetric under permutation of spins 1 and 2:

$$\begin{aligned} (12)|T_M m_S\rangle &= (+1)|T_M m_S\rangle, \\ (12)|S_0 m_S\rangle &= (-1)|S_0 m_S\rangle, \end{aligned} \quad (9)$$

where $M \in \{-1, 0, 1\}$ and the Zeeman eigen-equations are

$$\begin{aligned} (I_{1z} + I_{2z})|T_M m_S\rangle &= M|T_M m_S\rangle, \\ (I_{1z} + I_{2z})|S_0 m_S\rangle &= 0, \\ S_{3z}|T_M m_S\rangle &= m_S|T_M m_S\rangle, \\ S_{3z}|S_0 m_S\rangle &= m_S|S_0 m_S\rangle. \end{aligned} \quad (10)$$

The symbols α and β are used to denote $m_S = \pm \frac{1}{2}$ respectively. The symbol (12) indicates the permutation of the two I spins.

Consider the transition between the $|S_0 \beta\rangle$ and $|T_{-1} \alpha\rangle$ states, indicated in figure 1. This transition is “forbidden” since all off-diagonal matrix elements of the form $\langle S_0 \beta | (I_{1\mu} + I_{2\mu}) | T_{-1} \alpha \rangle$ are zero for $\mu \in \{x, y, z\}$. In fact, all Hamiltonian terms in equation 8 have a zero matrix element connecting these two states, except for the non-secular antisymmetric term H_D , with matrix elements given by

$$\langle S_0 \beta | H_D | T_{-1} \alpha \rangle = \langle T_{-1} \alpha | H_D | S_0 \beta \rangle = 2^{-1/2} \pi (J_{13} - J_{23}). \quad (11)$$

The difference between the corresponding diagonal elements of H_A is given by

$$\begin{aligned} \omega_{ST} &= \langle T_{-1} \alpha | H_A | T_{-1} \alpha \rangle - \langle S_0 \beta | H_A | S_0 \beta \rangle \\ &= B_{\text{bias}}(\gamma - \gamma_S) + \frac{\pi}{2}(4J_{12} - J_{13} - J_{23}), \end{aligned} \quad (12)$$

where the notation ω_{ST} indicates “singlet-triplet transition”. Note that this transition frequency includes a combination of I -spin and S -spin Larmor frequencies.

The term H_D induces a slight mixing of these two H_A eigenstates. The small degree of state mixing would have very little effect, if it were not for the time-dependence introduced by the coupling to the oscillating magnetic field, $H_{\text{WOLF}}(t)$. If the oscillation frequency matches the singlet-triplet transition frequency ($|\omega_{\text{WOLF}}| \simeq |\omega_{ST}|$), the periodic time-dependence drives coherent transitions between these two eigenstates. For example, suppose the initial state of the system consists of a strongly populated state $|S_0 \beta\rangle$, and a completely depleted state $|T_{-1} \alpha\rangle$. The density operator is described by

$$\begin{aligned} \langle S_0 \beta | \rho(0) | S_0 \beta \rangle &= 1, \\ \langle T_{-1} \alpha | \rho(0) | T_{-1} \alpha \rangle &= 0. \end{aligned} \quad (13)$$

Consider a WOLF pulse applied for a duration τ , on the resonance condition $\omega_{\text{WOLF}} = \omega_{ST}$. As discussed in more detail

in appendix A, the spin-state populations after the pulse are approximately given by

$$\begin{aligned} \langle S_0\beta | \rho(\tau) | S_0\beta \rangle &\simeq \frac{1}{2} (1 + \cos(\omega_{\text{nut}}^{ST} \tau)), \\ \langle T_{-1}\alpha | \rho(\tau) | T_{-1}\alpha \rangle &\simeq \frac{1}{2} (1 - \cos(\omega_{\text{nut}}^{ST} \tau)), \end{aligned} \quad (14)$$

where the singlet-triplet nutation frequency under the WOLF pulse is given by

$$\omega_{\text{nut}}^{ST} = 2\pi \sqrt{J_{13}^2 + J_{23}^2} \sin(\phi + \theta/2) J_1(A). \quad (15)$$

The angles θ and ϕ are given by

$$\begin{aligned} \theta &= \arctan 2(2J_{12}, J_{13} - J_{23}), \\ \phi &= \arctan 2(J_{13} + J_{23}, J_{13} - J_{23}), \end{aligned} \quad (16)$$

such that $\theta, \phi \ll 1$ in the near-equivalence regime.

The symbol J_1 denotes a Bessel function of the first kind with its argument given by

$$A = (\gamma_I - \gamma_S) B_{\text{WOLF}}^0 / \omega_{ST}. \quad (17)$$

These equations apply approximately in the limits $|J_{13} - J_{23}| \ll |J_{12}|$ and $J_{13}^2 + J_{23}^2 \ll \omega_{ST}^2$.

It is therefore possible to transport population completely from one state to the other by applying a WOLF pulse of duration $\pi / \omega_{\text{nut}}^{ST}$. The inversion speed is maximised by choosing the peak amplitude of the WOLF pulse to equal $B_{\text{WOLF}}^0 \simeq 2B_{\text{bias}}$, at which point the Bessel function $J_1(A)$ reaches its approximate maximum. Since there are practical limits on the generation of large oscillating magnetic fields, this technique is most appropriate for low-field magnetic resonance.

Note that an oscillating *transverse* field at the frequency ω_{WOLF} has negligible effect, since all matrix elements of the form $\langle \phi | I_{1x} + I_{2x} | \phi' \rangle$ are equal to zero, where $|\phi\rangle$ and $|\phi'\rangle$ are either $|S_0\beta\rangle$ or $|T_{-1}\alpha\rangle$.

The use of oscillating magnetic fields for the selective excitation of transitions has previously been explored in the context of ultralow-field NMR⁸. However, those experiments follow the familiar paradigm of resonant excitation, in which transitions are induced by modulating off-diagonal Hamiltonian terms at a frequency that matches the transition energy. In the current case, on the other hand, the off-diagonal non-secular terms are time-independent, and it is the diagonal terms that are given a periodic time-dependence by the oscillating applied field. There is a distant relationship with selective excitation in magic-angle-spinning solid-state NMR¹⁰.

B. Parahydrogen-induced polarization

The resonant driving of singlet-triplet transitions is particularly useful in the context of parahydrogen-induced polarization (PHIP), a technique which is widely used to enhance NMR signals^{11–29}. In this method, hydrogen gas is enriched in the *para* spin isomer and reacted with a substrate in the presence of a catalyst. The proton pair of the product molecule exhibits excess population in the singlet state. The strongly

enhanced singlet spin order is converted into hyperpolarized magnetization of heteronuclei such as ¹³C by applying a sequence of magnetic fields. A range of suitable techniques has been developed^{15–23,26,30,31}.

We now show that the application of a WOLF pulse in a small bias magnetic field leads to strong hyperpolarization of ¹³C nuclei in the reaction products of *para*-enriched H₂ gas, with potential advantages over other methods, as discussed below.

The principle of the experiment is shown in figure 1. The spin state populations (indicated by balls) are given for the case that the spins I_1 and I_2 are protons originating from the *para*-enriched hydrogen and the spin S_3 is a ¹³C nucleus in the product molecule. The populations of the $|S_0\alpha\rangle$ and $|S_0\beta\rangle$ states are strongly enhanced due to their provenance as the nuclei of the *para*-enriched H₂ spin isomer. Since these two populations are equal there is no polarization of the S -spin at this stage. However, if the WOLF pulse transports the population from the $|S_0\beta\rangle$ state to the $|T_{-1}\alpha\rangle$ state, as shown in equation 14, the resulting population distribution has excess population in the $|S_0\alpha\rangle$ and $|T_{-1}\alpha\rangle$ states. Since the S -spin is in the state $|\alpha\rangle$ in both cases, this corresponds to a high degree of ¹³C polarization. A ¹³C polarization of the order of unity represents an enhancement of the ¹³C NMR signals by around 5 orders of magnitude, relative to ordinary NMR based on thermal equilibrium polarization in a strong magnetic field.

We propose the acronym WEREWOLF (Whopping Enhancement Realised by Excitation With Oscillating Low Fields) for *para*-hydrogen-induced polarization of heteronuclei using WOLF pulses for the singlet-triplet population transfer.

TABLE I. Spin-spin coupling parameters for (1-¹³C)fumarate and (1-¹³C)maleate, adapted from reference¹⁹.

Compound	J_{12} (Hz)	J_{23} (Hz)	J_{13} (Hz)
Fumarate	15.9	5.8	3.3
Maleate	12.3	12.9	2.5

III. METHODS

A. Materials

The substances fumarate (*E*-butenedioate) and maleate (*Z*-butenedioate) were used for demonstrations of WEREWOLF. The chemical structures are shown in figure 2. The precursor solution for fumarate was prepared by dissolving 100 mM disodium acetylene dicarboxylate, 100 mM sodium sulfite, and 6 mM [RuCp*(MeCN)₃]PF₆ (CAS number: 99604-67-8) in D₂O, heating to 60°C, and passing through a Millex® 0.22 μm PES filter.

The precursor solution for maleate was prepared by dissolving 100 mM acetylene dicarboxylic acid and 5 mM [Rh(dppb)(COD)]BF₄ (CAS number: 7440-16-6) in methanol-d₄. All materials and consumables were purchased from Merck.

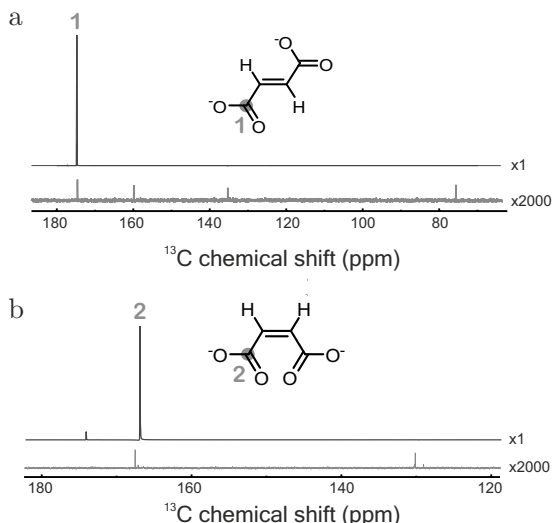


FIG. 2. ^1H -decoupled ^{13}C spectra of (a) fumarate and (b) maleate at a field of 9.41 T. Single-transient WEREWOLF-hyperpolarized ^{13}C spectra are compared with conventional ^{13}C NMR spectra acquired at thermal equilibrium, averaged over 360 transients (for fumarate) or 512 transients (for maleate). The strong ^{13}C peaks are from hyperpolarized naturally occurring ^{13}C nuclei at the molecular sites indicated by filled circles. The ^{13}C peaks at 160 ppm and 76 ppm in (a) correspond to unreacted disodium acetylene dicarboxylate. The small signal at 172 ppm in (b) is attributed to succinate generated by secondary hydrogenation. The change in chemical shift for the maleate ^{13}C peak in (b) is provisionally attributed to a change in sample temperature.

Para-enriched hydrogen was produced by passing hydrogen gas over an iron oxide catalyst packed in 1/4 inch stainless steel tube and cooled by liquid nitrogen.

Under the reaction and solvent conditions used for the experiments, maleate is expected to exist mainly in the form of the protonated singly-charged mono-hydrogen maleate anion, while fumarate is expected to exist as the doubly-charged non-protonated fumarate anion. These protonation states are ignored in the current report, for the sake of simplicity.

About 2% of fumarate and maleate molecules contain a naturally-occurring ^{13}C nucleus at the sites shown in figure 2. The two ^1H nuclei and the ^{13}C nucleus form a three-spin-1/2 system of the type discussed above. The J -coupling parameters for the two molecular systems are given in table I.

B. Equipment

A sketch of the equipment is shown in figure 3. The hydrogen gas is bubbled through the solutions using a 1/16 inch PEEK capillary tube inserted inside a thin-walled Norell@ pressure NMR tube. The Rheodyne MXP injection valves and the Keysight 33500B waveform generator were triggered and controlled by an Arduino Mega 2560 micro-controller board. The waveform generator was connected to the 3 cm wide and 30 cm long solenoid coil of 300 turns placed in a TwinLeaf MS-4 mu-metal shield and used for generating the

oscillating magnetic field. The bias field was generated by the built-in Helmholtz coil of the Twinleaf shield, powered by a Keithley 6200 DC current source. A ~ 200 turn solenoid guide coil was wound around the orifice penetrating the mu-metal shield and continuously driven by a second Keithley 6200 DC current source to produce $6 \mu\text{T}$ field. The guide coil was used to avoid zero-field crossings during sample transportation¹⁰.

C. Experimental Procedure

Figure 4 shows a timing diagram of the WEREWOLF experiment, showing the magnetic fields experienced by the sample as a function of time. Each experiment starts by warming $250 \mu\text{L}$ of the sample mixture to $\sim 90^\circ\text{C}$ in the ambient magnetic field of the laboratory ($\sim 110 \mu\text{T}$), followed by insertion into the magnetic shield. *Para*-enriched hydrogen gas is bubbled through the solution at 6 bar pressure. The bubbling time τ_b was set to 30 s and 10 s for experiments involving fumarate and maleate, respectively. The oscillating WOLF pulse is applied for an interval τ in the presence of a bias field of $B_{\text{bias}} = 2 \mu\text{T}$. For the experiments shown here the WOLF pulse was arbitrarily set to $B_{\text{WOLF}}^0 = 2 \mu\text{T}$, which is one half of its optimal value according to theory. At the end of the WOLF pulse the bias field is increased for a few seconds, and the sample manually removed from the shield and inserted by hand into the 9.41 T NMR magnet.

The ^{13}C free-induction decays were excited by a hard pulse of 14.7 kHz rf amplitude and recorded with 65 k point density at the spectral width of 200 ppm using a Bruker Avance Neo spectrometer. Additional ^1H decoupling was used for all experiments. Thermal equilibrium ^{13}C spectra were recorded at room temperature with recycle delays of 120 s, averaging the signals from 512 and 360 transients for maleate and sodium fumarate, respectively.

IV. RESULTS

Figure 2 shows single-transient hyperpolarized ^{13}C NMR spectra for (a) fumarate and (b) maleate, obtained using the WEREWOLF procedure. The WOLF pulse parameters were $\omega_{\text{WOLF}}/2\pi = 77.3 \text{ Hz}$ and $\tau = 0.65 \text{ s}$ for fumarate, and $\omega_{\text{WOLF}}/2\pi = 74.0 \text{ Hz}$ and $\tau = 0.12 \text{ s}$ for maleate.

Conventional ^{13}C NMR spectra obtained by multiple signal acquisitions on the hydrogenated samples after thermal equilibration are also shown in figure 2. Comparison of these spectra allows the estimation of the ^{13}C polarization levels achieved by WEREWOLF, which are $p \simeq 8\%$ for fumarate and $p \simeq 19\%$ for maleate. These results are highly competitive with previous work^{28,31,33,34}, especially when the relatively low *para*-hydrogen enrichment levels, crude apparatus, manual sample transport, and sub-optimal reaction conditions are taken into account.

Integrated ^{13}C signal amplitudes as a function of the WOLF pulse duration τ are shown in figure 5. The coherent oscillations of the hyperpolarized magnetization are striking. Each experimental point was obtained from a separate experiment

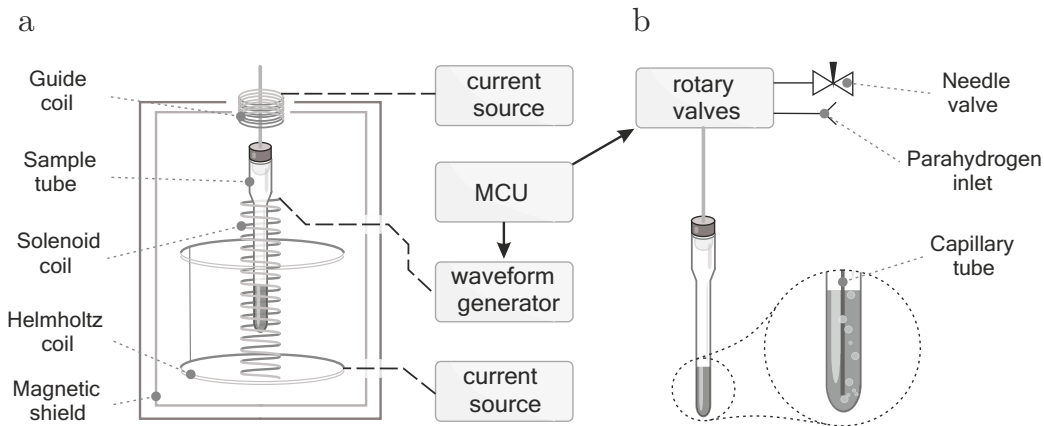


FIG. 3. Schematic diagram of the experimental setup. (a) Mu-metal shield and associated components. During the WOLF pulse, the Helmholtz coil generates the bias field B_{bias} whereas the solenoid coil produces the oscillating field $B_{\text{WOLF}}(t)$ (b) Gas-handling apparatus including a thick-wall NMR tube equipped with a capillary for the *para*-enriched H₂ gas. MCU - micro-controller unit.

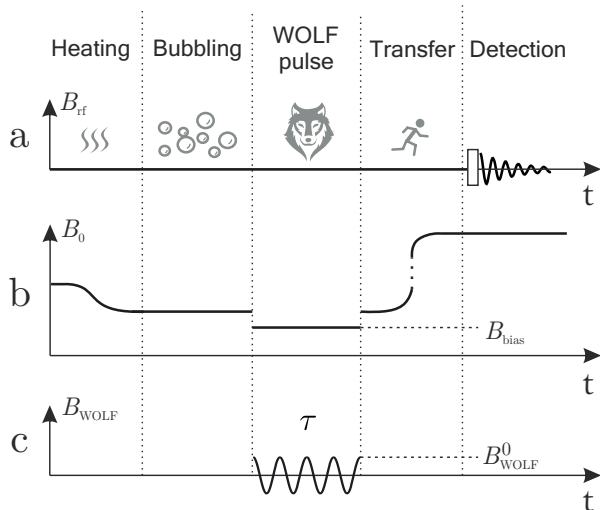


FIG. 4. Timing diagram for the WEREWOLF procedure, involving bubbling of the sample with *para*-enriched hydrogen gas and a sequence of magnetic fields. (a) ^{13}C radio-frequency pulse applied in high magnetic field at the end of the procedure and NMR signal acquisition. (b) Magnetic field along the z -axis, showing the ambient laboratory field during sample heating, the reduction in field as the sample is placed in the shield, the bias field B_{bias} during the WOLF pulse, the removal of the sample from the shield and insertion into the high-field NMR magnet. (c) Oscillating WOLF pulse field, applied for a duration τ , with a frequency ω_{WOLF} and peak amplitude B_{WOLF}^0 . The total field experienced by the sample is the sum of (b) and (c).

on a fresh sample. The normalized experimental data is compared with numerical simulations and analytical curves derived from equations 14 and 15. The agreement between both curves and the experimental data is gratifying. The oscillations are much faster for maleate than for fumarate, mainly

because the difference in heteronuclear J-couplings is 10.4 Hz for maleate but only 2.5 Hz for fumarate (see table I).

As discussed in section II A the singlet-triplet transition is effectively driven once the condition $\omega_{\text{WOLF}} = \omega_{ST}$ is fulfilled. This is evident in Fig. 6 which displays hyperpolarized ^{13}C signal intensity as a function of ω_{WOLF} at fixed WOLF pulse duration. The experimental data points indicate a sharp resonance for fumarate with full-width-at-half-maximum (FWHM) of ~ 0.4 Hz whereas a larger FWHM of ~ 6 Hz is observed for maleate. The experimental frequency profiles match well the numerical simulations indicated by solid lines. The good agreement indicates that the effects of field inhomogeneity were minor in this case.

V. CONCLUSIONS

Magnetic resonance phenomena involving non-secular spin-spin couplings are normally encountered in systems with large nuclear quadrupolar couplings² or hyperfine couplings to unpaired electrons, as in solid-effect dynamic nuclear polarization (DNP)³ and stimulated nuclear polarization in photochemical reactions involving transient radical pairs⁴. The work described here shows that non-secular out-of-pair couplings may also be exploited in purely nuclear spin systems, albeit at an energy scale which is ~ 9 orders of magnitude lower than in solid-effect DNP. Here too, non-secular effects allow “forbidden” transitions to couple to the electromagnetic field, allowing the generation of strong nuclear hyperpolarization.

Many other methods have been described for the transformation of ^1H singlet order to ^{13}C magnetization, including pulse techniques^{15–19}, field-cycling and level-anticrossing phenomena^{20–23}, and low-field methods^{22–25,29,30}. However most of these schemes are active either in the “ultralow field” regime (Larmor frequencies less than or comparable to J-couplings), or the “high-field” regime of conventional NMR

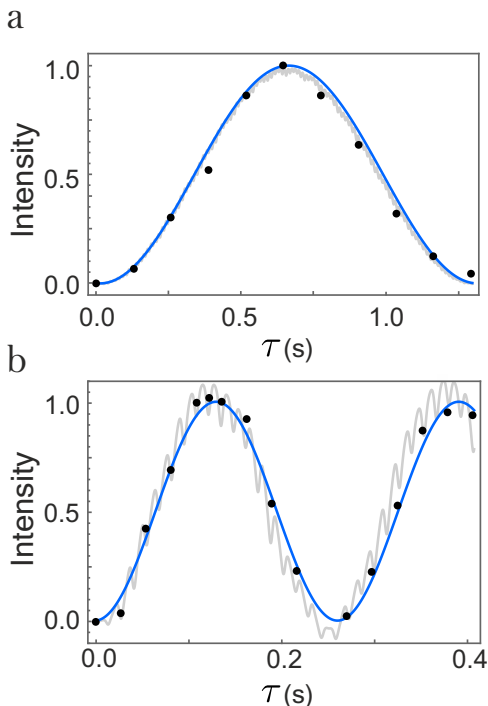


FIG. 5. Hyperpolarized fumarate (a) and maleate (b) ^{13}C signal intensities as a function of the WOLF pulse duration τ . The WOLF pulse frequencies are 77.3 Hz for fumarate and 74.0 Hz for maleate. The black dots depict integrated experimental signal amplitudes, normalized to 1 for the maximum value. The grey lines represent numerical *SpinDynamica*³² simulations for the coupling parameters in table I. The blue lines show analytical solutions given by equation 14. All values of τ used for the experiments are integer numbers of the WOLF period $2\pi/\omega_{\text{WOLF}}$, which is 12.94 ms for fumarate and 13.51 ms for maleate.

spectroscopy. Both of these regimes are associated with some disadvantages: The ultralow field regime is associated with short coherence lifetimes through couplings to quadrupolar nuclear isotopes²⁷ such as ^2H and ^{14}N , while the high-field regime of conventional NMR is associated with singlet-triplet conversion of the dissolved *para*-hydrogen gas, leading to reduced polarization levels of the product molecules^{33,35,36}.

The WOLF method described here provides a fast exchange of singlet and triplet populations. The bias field is conveniently applied in the same direction as the WOLF pulse and may in principle be set to any value, within technical constraints. A small bias field of a few μT is sufficient to resolve the Larmor frequencies of the different nuclear isotopes. In principle, this should make it possible to implement heteronuclear spin decoupling by resonant transverse oscillating fields. Furthermore, the coherent nature of the singlet-triplet conversion should allow deployment of the full palette of “pulse tricks” developed for conventional high-field NMR, including error-compensating composite pulses³⁷. Applications are envisaged to other hyperpolarization techniques, such as the SABRE (Signal Amplification by Reversible Exchange) method^{13,26}. The method described here might be related to

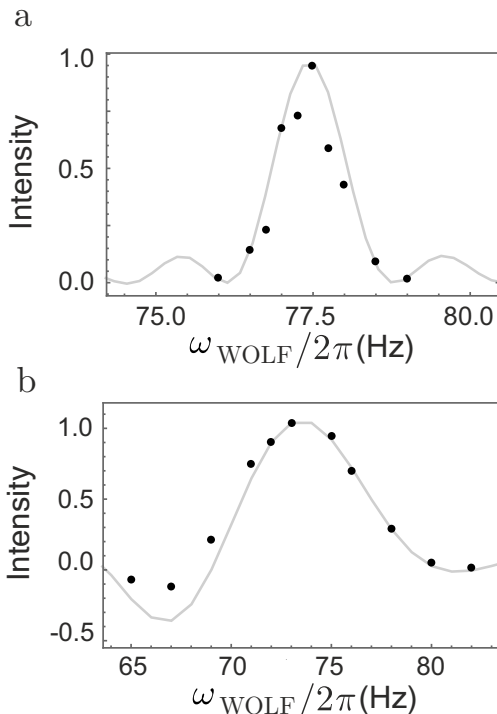


FIG. 6. Hyperpolarised fumarate (a) and maleate (b) ^{13}C signal intensity as a function of WOLF pulse frequency ω_{WOLF} . The pulse duration τ is set to 0.65 s for fumarate and 0.12 s for maleate. The black dots depict integrated experimental signal amplitudes, normalized to 1 for the maximum value. The grey lines represent numerical *SpinDynamica*³² simulations for the coupling parameters in table I.

some recent variants of SABRE which also use periodically modulated magnetic fields^{24,29}.

ACKNOWLEDGMENTS

We acknowledge funding received by the Marie Skłodowska-Curie program of the European Union (grant number 766402), the European Research Council (grant 786707-FunMagResBeacons), and EPSRC-UK (grants EP/P009980/1, EP/P030491/1, EP/V055593/1). We thank Soumya Singha Roy for discussions, and Marcel Utz and Andrey Pravdivtsev for comments on the manuscript. We thank Weidong Gong for instrumental help, and one of the referees for bringing stimulated nuclear polarization to our attention⁴.

AUTHOR DECLARATIONS

Conflict of interest

The authors have no conflicts to disclose.

DATA AVAILABILITY STATEMENT

The data that support the findings of this study are available from the corresponding author upon reasonable request.

Appendix A: WOLF pulse dynamics

The complete Hamiltonian given by equation 7 preserves the total z -angular momentum of the system

$$[H(t), I_{1z} + I_{2z} + S_{3z}] = 0. \quad (\text{A1})$$

$$[H(t)]_W = \begin{bmatrix} \frac{1}{2}(B(t)\gamma_S - 3\pi J_{12}) & \frac{\pi}{2}(J_{23} - J_{13}) & \frac{\pi}{\sqrt{2}}(J_{13} - J_{23}) \\ \frac{\pi}{2}(J_{23} - J_{13}) & \frac{1}{2}(B(t)\gamma_S + \pi J_{12}) & \frac{\pi}{\sqrt{2}}(J_{13} + J_{23}) \\ \frac{\pi}{\sqrt{2}}(J_{13} - J_{23}) & \frac{\pi}{\sqrt{2}}(J_{13} + J_{23}) & (\gamma_I - \frac{1}{2}\gamma_S)B(t) + \frac{\pi}{2}(J_{12} - J_{13} - J_{23}) \end{bmatrix}, \quad (\text{A3})$$

where

$$B(t) = B_{\text{bias}} + B_{\text{WOLF}}^0 \cos(\omega_{\text{WOLF}} t). \quad (\text{A4})$$

Although small, the mixing between the states $|S_0\alpha\rangle$ and $|T_0\alpha\rangle$ is not negligible during the WOLF pulse dynamics. To

In the near-equivalence regime the matrix representation of $H(t)$ restricted to W_θ is given by

$$[H(t)]_{W_\theta} \simeq \begin{bmatrix} \frac{1}{2}(B(t)\gamma_S - 3\pi J_{12}) & 0 & \frac{\pi}{\sqrt{2}}(\cos(\theta/2)(J_{13} - J_{23}) + \sin(\theta/2)(J_{13} + J_{23})) \\ 0 & \frac{1}{2}(B(t)\gamma_S + \pi J_{12}) & \frac{\pi}{\sqrt{2}}(\cos(\theta/2)(J_{13} + J_{23}) - \sin(\theta/2)(J_{13} - J_{23})) \\ \blacksquare & \blacksquare & (\gamma_I - \frac{1}{2}\gamma_S)B(t) + \frac{\pi}{2}(J_{12} - J_{13} - J_{23}) \end{bmatrix}, \quad (\text{A7})$$

where the black squares should be replaced by the elements on the opposite side of the diagonal, so that the matrix is invariant under transposition.

According to equation A7 the transition frequency between states $|S'_0\beta\rangle$ and $|T'_{-1}\alpha\rangle$ in the near-equivalence regime is given by

$$\begin{aligned} \omega_{ST} &= \langle T'_{-1}\alpha | H_0 | T'_{-1}\alpha \rangle - \langle S'_0\beta | H_0 | S'_0\beta \rangle \\ &= B_{\text{bias}}(\gamma_I - \gamma_S) + \frac{\pi}{2}(4J_{12} - J_{13} - J_{23}), \end{aligned} \quad (\text{A8})$$

whereas the transition frequency between $|T'_0\beta\rangle$ and $|T'_{-1}\alpha\rangle$ is

This suggests that the basis states highlighted in figure 1 separate the matrix representation of $H(t)$ into two 3×3 and two 1×1 blocks. The 1×1 blocks may be disregarded, the 3×3 blocks are generated by the sets

$$\begin{aligned} V &= \{|S_0\alpha\rangle, |T_0\alpha\rangle, |T_{+1}\beta\rangle\}, \\ W &= \{|S_0\beta\rangle, |T_0\beta\rangle, |T_{-1}\alpha\rangle\}. \end{aligned} \quad (\text{A2})$$

The standard WEREWOLF experiment (Fig. 4) aims to create positive heteronuclear magnetisation which may be achieved through a population swap of states $|S_0\beta\rangle$ and $|T_{-1}\alpha\rangle$. We thus consider the restriction of $H(t)$ to W , which may be explicitly given as follows

account for the mixing we define a set of rotated basis states

$$\begin{aligned} W_\theta &= \{|S'_0\beta\rangle, |T'_0\beta\rangle, |T'_{-1}\alpha\rangle\} \\ &= \{\cos(\theta/2)|S_0\beta\rangle + \sin(\theta/2)|T_0\beta\rangle, \\ &\quad \cos(\theta/2)|T_0\beta\rangle - \sin(\theta/2)|S_0\beta\rangle, |T_{-1}\alpha\rangle\}, \end{aligned} \quad (\text{A5})$$

parameterised by the angle θ . The angle θ is chosen to satisfy

$$\theta = \arctan2(2J_{12}, J_{13} - J_{23}). \quad (\text{A6})$$

given by

$$\begin{aligned} \omega_{TT} &= \langle T'_{-1}\alpha | H_0 | T'_{-1}\alpha \rangle - \langle S'_0\beta | H_0 | S'_0\beta \rangle \\ &= B_{\text{bias}}(\gamma_I - \gamma_S) - \frac{\pi}{2}(J_{13} + J_{23}). \end{aligned} \quad (\text{A9})$$

Application of a WOLF pulse with $\omega_{\text{WOLF}} = \omega_{ST}$ causes a resonant modulation of the energy difference between states $|S'_0\beta\rangle$ and $|T'_{-1}\alpha\rangle$, but causes an off-resonant modulation of the energy difference between states $|T'_0\beta\rangle$ and $|T'_{-1}\alpha\rangle$ on the order of $\sim J_{12}$. To a first approximation we may neglect the

state $|T'_0\beta\rangle$ altogether, and consider a fictitious two-level sys-

$$h(t) = \begin{bmatrix} \langle S'_0\beta|H(t)|S'_0\beta\rangle & \langle S'_0\beta|H(t)|T'_{-1}\alpha\rangle \\ \langle T'_{-1}\alpha|H(t)|S'_0\beta\rangle & \langle T'_{-1}\alpha|H(t)|T'_{-1}\alpha\rangle \end{bmatrix} \\ = \begin{bmatrix} \frac{1}{2}(B(t)\gamma_S - 3\pi J_{12}) & \frac{\pi}{\sqrt{2}}(\cos(\theta/2)(J_{13} - J_{23}) + \sin(\theta/2)(J_{13} + J_{23})) \\ \frac{\pi}{\sqrt{2}}(\cos(\theta/2)(J_{13} - J_{23}) + \sin(\theta/2)(J_{13} + J_{23})) & (\gamma_I - \frac{1}{2}\gamma_S)B(t) + \frac{\pi}{2}(J_{12} - J_{13} - J_{23}) \end{bmatrix}. \quad (\text{A10})$$

In terms of *normalised* Pauli matrices ($\sigma_j/2$) the Hamiltonian $h(t)$ may be expressed as shown below

$$h(t) = \omega_0\sigma_0 + \omega_x\sigma_x/2 + \omega_z(t)\sigma_z/2, \quad (\text{A11})$$

with

$$\omega_0 = \frac{1}{2}\gamma_I(B_{\text{bias}} + B_{\text{WOLF}}^0 \cos(\omega_{ST}t)) - \frac{\pi}{4}(2J_{12} + J_{13} + J_{23}), \\ \omega_x = \pi\sqrt{2}(\cos(\theta/2)(J_{13} - J_{23}) + \sin(\theta/2)(J_{13} + J_{23})), \\ \omega_z(t) = -B_{\text{WOLF}}^0(\gamma_I - \gamma_S)\cos(\omega_{ST}t) - \omega_{ST}. \quad (\text{A12})$$

The Pauli coefficient ω_x may alternatively be expressed as follows

$$\omega_x = 2\pi\sqrt{J_{13}^2 + J_{23}^2}\sin(\phi + \theta/2), \\ \phi = \arctan2(J_{13} + J_{23}, J_{13} - J_{23}), \quad (\text{A13})$$

where we made use of the following relations

$$\sqrt{J_{13} + J_{23}}\sin(\phi) = (J_{13} - J_{23})/\sqrt{2}, \\ \sqrt{J_{13} + J_{23}}\cos(\phi) = (J_{13} + J_{23})/\sqrt{2}. \quad (\text{A14})$$

Within our approximations the ω_0 -term introduces an overall phase shift and may be discarded. The WOLF pulse dynamics may now be approximately described within a ‘‘jolting’’ interaction frame¹⁰. The jolting frame represents a rotating frame with a time-dependent rotation frequency. The time-dependent rotation frequency and the rotation angle $\psi(t)$ are related as follows

$$\psi(t) = \int_0^t \omega_z(s)ds. \quad (\text{A15})$$

The jolting frame Hamiltonian $\tilde{h}(t)$ is then given by

$$\tilde{h}(t) = \frac{\omega_x}{2}\exp(+i\psi(t)\sigma_z/2)\sigma_x\exp(-i\psi(t)\sigma_z/2) \\ = \frac{\omega_x}{4}(\exp(+i\psi(t))\sigma_+ + \exp(-i\psi(t))\sigma_-). \quad (\text{A16})$$

We may expand the jolting frame Hamiltonian as a Fourier series

$$\tilde{h}(t) = \frac{\omega_x}{4}\left(\sum_n J_n(A)\exp(-i(n-1)\omega_{ST}t)\sigma_+ + \sum_n J_{-n}(A)\exp(-i(n+1)\omega_{ST}t)\sigma_-\right), \quad (\text{A17})$$

tem evolving under the Hamiltonian $h(t)$

where $J_n(x)$ is the n 'th Bessel function of the first kind and the argument A is defined as follows

$$A = (\gamma_I - \gamma_S)B_{\text{WOLF}}^0/\omega_{ST}. \quad (\text{A18})$$

For $|\omega_x/\omega_{ST}| \ll 1$, which is bounded from above by

$$|\omega_x/\omega_{ST}| \leq 2\pi\sqrt{J_{13}^2 + J_{23}^2}/|\omega_{ST}|, \quad (\text{A19})$$

we may neglect the time-dependent terms of $\tilde{h}(t)$. This approach is equivalent to truncating the average Hamiltonian after first order³⁸

$$\tilde{h}(t) \simeq \frac{\omega_x}{4}(J_1(A)\sigma_+ + J_1(A)\sigma_-), \\ = \omega_x J_1(A)\sigma_x/2. \quad (\text{A20})$$

The effective nutation frequency of a WOLF pulse is thus given by

$$\omega_{\text{nut}}^{ST} = \omega_x J_1(A) = 2\pi\sqrt{J_{13}^2 + J_{23}^2}\sin(\phi + \theta/2)J_1(A). \quad (\text{A21})$$

¹R. R. Ernst, G. Bodenhausen, and A. Wokaun, *Principles of Nuclear Magnetic Resonance in One and Two Dimensions* (Clarendon Press, Oxford, 1987).

²R. Tycko and S. J. Opella, ‘‘Overtone NMR spectroscopy,’’ *J. Chem. Phys.* **86**, 1761–1774 (1987).

³W. T. Wenckebach, ‘‘The Solid Effect,’’ *Appl. Magn. Reson.* **34**, 227–235 (2008).

⁴R. Z. Sagdeev and E. G. Bagryanskaya, ‘‘Stimulated nuclear polarization - a new method for studying the mechanisms of photochemical reactions,’’ *Pure Appl. Chem.* **62**, 1547–1556 (1990).

⁵J. W. Blanchard, T. F. Sjolander, J. P. King, M. P. Ledbetter, E. H. Levine, V. S. Bajaj, D. Budker, and A. Pines, ‘‘Measurement of untruncated nuclear spin interactions via zero- to ultralow-field nuclear magnetic resonance,’’ *Phys. Rev. B* **92**, 220202 (2015).

⁶R. L. Hesketh and K. M. Brindle, ‘‘Magnetic resonance imaging of cancer metabolism with hyperpolarized ¹³C-labeled cell metabolites,’’ *Current Opinion in Chemical Biology Molecular Imaging / Chemical Genetics and Epigenetics*, **45**, 187–194 (2018).

⁷G. Pileio, M. Carravetta, and M. H. Levitt, ‘‘Extremely Low-Frequency Spectroscopy in Low-Field Nuclear Magnetic Resonance,’’ *Phys. Rev. Letters* **103**, 083002 (2009).

⁸T. F. Sjolander, M. C. D. Tayler, J. P. King, D. Budker, and A. Pines, ‘‘Transition-Selective Pulses in Zero-Field Nuclear Magnetic Resonance,’’ *J. Phys. Chem. A* **120**, 4343–4348 (2016).

⁹M. C. D. Tayler and M. H. Levitt, ‘‘Singlet nuclear magnetic resonance of nearly-equivalent spins,’’ *Phys. Chem. Chem. Phys.* **13**, 5556–5560 (2011).

¹⁰P. Caravatti, G. Bodenhausen, and R. R. Ernst, ‘‘Selective pulse experiments in high-resolution solid state NMR,’’ *J. Magn. Reson.* **55**, 88–103 (1983).

- ¹¹C. R. Bowers and D. P. Weitekamp, "Transformation of Symmetrization Order to Nuclear-Spin Magnetization by Chemical Reaction and Nuclear Magnetic Resonance," *Phys. Rev. Lett.* **57**, 2645–2648 (1986).
- ¹²C. R. Bowers and D. P. Weitekamp, "Parahydrogen and synthesis allow dramatically enhanced nuclear alignment," *J. Am. Chem. Soc.* **109**, 5541–5542 (1987).
- ¹³R. W. Adams, J. A. Aguilar, K. D. Atkinson, M. J. Cowley, P. I. P. Elliott, S. B. Duckett, G. G. R. Green, I. G. Khazal, J. Lopez-Serrano, and D. C. Williamson, "Reversible Interactions with para-Hydrogen Enhance NMR Sensitivity by Polarization Transfer," *Science* **323**, 1708–1711 (2009).
- ¹⁴B. Ripka, J. Eills, H. Kouřilová, M. Leutzsch, M. H. Levitt, and K. Münnemann, "Hyperpolarized fumarate via parahydrogen," *Chem. Commun.* **54**, 12246–12249 (2018).
- ¹⁵M. Goldman and H. Jóhannesson, "Conversion of a proton pair para order into ¹³C polarization by rf irradiation, for use in MRI," *Comptes Rendus Physique* **6**, 575–581 (2005).
- ¹⁶S. Kadlecěk, K. Emami, M. Ishii, and R. Rizi, "Optimal transfer of spin-order between a singlet nuclear pair and a heteronucleus," *J. Magn. Reson.* **205**, 9–13 (2010).
- ¹⁷T. Theis, M. Truong, A. M. Coffey, E. Y. Chekmenev, and W. S. Warren, "LIGHT-SABRE enables efficient in-magnet catalytic hyperpolarization," *J. Magn. Reson.* **248**, 23–26 (2014).
- ¹⁸J. Eills, G. Stevanato, C. Bengs, S. Glöggler, S. J. Elliott, J. Alonso-Valdesueiro, G. Pileio, and M. H. Levitt, "Singlet order conversion and parahydrogen-induced hyperpolarization of ¹³C nuclei in near-equivalent spin systems," *J. Magn. Reson.* **274**, 163–172 (2017).
- ¹⁹C. Bengs, L. Dagys, and M. H. Levitt, "Robust transformation of singlet order into heteronuclear magnetisation over an extended coupling range," *Journal of Magnetic Resonance* **321**, 106850 (2020).
- ²⁰H. Jóhannesson, O. Axelsson, and M. Karlsson, "Transfer of parahydrogen spin order into polarization by diabatic field cycling," *Comptes Rendus Phys. Highly Polarized Nuclear Spin Systems and Dipolar Interactions in NMR*, **5**, 315–324 (2004).
- ²¹A. N. Pravdivtsev, A. V. Yurkovskaya, N. N. Lukzen, K. L. Ivanov, and H.-M. Vieth, "Highly Efficient Polarization of Spin-1/2 Insensitive NMR Nuclei by Adiabatic Passage through Level Anticrossings," *J. Phys. Chem. Lett.* **5**, 3421–3426 (2014).
- ²²T. Theis, M. L. Truong, A. M. Coffey, R. V. Shchepin, K. W. Waddell, F. Shi, B. M. Goodson, W. S. Warren, and E. Y. Chekmenev, "Microtesla SABRE Enables 10% Nitrogen-15 Nuclear Spin Polarization," *J. Am. Chem. Soc.* **137**, 1404–1407 (2015).
- ²³J. Eills, J. W. Blanchard, T. Wu, C. Bengs, J. Hollenbach, D. Budker, and M. H. Levitt, "Polarization transfer via field sweeping in parahydrogen-enhanced nuclear magnetic resonance," *J. Chem. Phys.* **150**, 174202 (2019).
- ²⁴J. R. Lindale, S. L. Eriksson, C. P. N. Tanner, Z. Zhou, J. F. P. Colell, G. Zhang, J. Bae, E. Y. Chekmenev, T. Theis, and W. S. Warren, "Unveiling coherently driven hyperpolarization dynamics in signal amplification by reversible exchange," *Nat Commun* **10**, 1–7 (2019).
- ²⁵C. P. N. Tanner, J. R. Lindale, S. L. Eriksson, Z. Zhou, J. F. P. Colell, T. Theis, and W. S. Warren, "Selective hyperpolarization of heteronuclear singlet states via pulsed microtesla SABRE," *J. Chem. Phys.* **151**, 044201 (2019).
- ²⁶D. A. Barskiy, S. Knecht, A. V. Yurkovskaya, and K. L. Ivanov, "SABRE: Chemical kinetics and spin dynamics of the formation of hyperpolarization," *Progress in Nuclear Magnetic Resonance Spectroscopy* **114–115**, 33–70 (2019).
- ²⁷J. R. Birchall, M. S. H. Kabir, O. G. Salnikov, N. V. Chukanov, A. Svyatova, K. V. Kovtunov, I. V. Koptuyug, J. G. Gelovani, B. M. Goodson, W. Pham, and E. Y. Chekmenev, "Quantifying the effects of quadrupolar sinks via ¹⁵N relaxation dynamics in metronidazoles hyperpolarized via SABRE-SHEATH," *Chem. Commun.* **56**, 9098–9101 (2020).
- ²⁸S. Knecht, J. W. Blanchard, D. Barskiy, E. Cavallari, L. Dagys, E. V. Dyke, M. Tsukanov, B. Bliemel, K. Münnemann, S. Aime, F. Reineri, M. H. Levitt, G. Buntkowsky, A. Pines, P. Blümler, D. Budker, and J. Eills, "Rapid hyperpolarization and purification of the metabolite fumarate in aqueous solution," *PNAS* **118** (2021).
- ²⁹S. L. Eriksson, J. R. Lindale, X. Li, and W. S. Warren, "Improving SABRE hyperpolarization with highly non-intuitive pulse sequences: Moving beyond avoided crossings to describe dynamics," *ArXiv:210704687 Phys.* (2021), arXiv:2107.04687 [physics].
- ³⁰S. J. DeVience, M. Greer, S. Mandal, and M. S. Rosen, "Homonuclear J-Coupling Spectroscopy at Low Magnetic Fields using Spin-Lock Induced Crossing," *ArXiv:210301289 Phys.* (2021), arXiv:2103.01289 [physics].
- ³¹L. Wienands, F. Theiß, J. Eills, L. Rösler, S. Knecht, and G. Buntkowsky, "Optimizing the Reaction Conditions for the Formation of Fumarate via Trans-Hydrogenation," *Appl Magn Reson*, 1–20 (2021).
- ³²C. Bengs and M. H. Levitt, "SpinDynamica: Symbolic and numerical magnetic resonance in a Mathematica environment," *Magn. Reson. Chem.* **56**, 374–414 (2018).
- ³³B. A. Rodin, J. Eills, R. Picazo-Frutos, K. F. Sheberstov, D. Budker, and K. L. Ivanov, "Constant-adiabaticity ultralow magneticfield manipulations of parahydrogen-induced polarization: Application to an AA'X spin system," *Phys. Chem. Chem. Phys.* **23**, 7125–7134 (2021).
- ³⁴B. A. Rodin, V. P. Kozinenko, A. S. Kiryutin, A. V. Yurkovskaya, J. Eills, and K. L. Ivanov, "Constant-adiabaticity pulse schemes for manipulating singlet order in 3-spin systems with weak magnetic non-equivalence," *J. Magn. Reson.* **327**, 106978–106978 (2021).
- ³⁵S. Knecht, A. S. Kiryutin, A. V. Yurkovskaya, and K. L. Ivanov, "Mechanism of spontaneous polarization transfer in high-field SABRE experiments," *Journal of Magnetic Resonance* **287**, 74–81 (2018).
- ³⁶S. Knecht, S. Hadjiali, D. A. Barskiy, A. Pines, G. Sauer, A. S. Kiryutin, K. L. Ivanov, A. V. Yurkovskaya, and G. Buntkowsky, "Indirect Detection of Short-Lived Hydride Intermediates of Iridium N-Heterocyclic Carbene Complexes via Chemical Exchange Saturation Transfer Spectroscopy," *J. Phys. Chem. C* **123**, 16288–16293 (2019).
- ³⁷M. H. Levitt, "Composite pulses," *Progress in Nuclear Magnetic Resonance Spectroscopy* **18**, 61–122 (1986).
- ³⁸U. Haeberlen and J. S. Waugh, "Coherent Averaging Effects in Magnetic Resonance," *Phys. Rev.* **175**, 453 (1968).